

3D PRINTING AND ADDITIVE MANUFACTURING Volume 7, Number 6, 2020 © Mary Ann Liebert, Inc. DOI: 10.1089/3dp.2019.0160

ORIGINAL ARTICLE

A Radiopaque Nanoparticle-Based Ink Using PolyJet 3D Printing for Medical Applications

Alice Shannon,¹ Aine O'Connell,² Aidan O'Sullivan,^{1,3} Michael Byrne,⁴ Seamus Clifford,⁴ Kevin J. O'Sullivan,^{1,3} and Leonard O'Sullivan^{1,3}

Abstract

The aim of this study was to develop a 3D printable radiopaque ink and successfully print a finished artifact. Radiopaque 3D printing would be hugely beneficial to improve the visibility of medical devices and implants, as well as allowing more realistic phantoms and calibration aids to be produced. Most 3D printing technologies are polymer based. Polymers are naturally radiolucent, allowing X-rays to pass through, showing up as faint dark gray regions on X-ray detectors, as for soft tissues. During this study, a 3D printable ultraviolet (UV) curable resin containing zirconium oxide (ZrO₂) nanoparticles was developed. 5 wt.% ZrO₂ was dispersed in a base resin using a high-shear mixer. Particles remained in suspension for 6–8 h at room temperature, allowing time for 3D printing. A model of a hand including radiopaque bones and a test block demonstrating a range of internal radiopaque features were successfully 3D printed. Radiopacity was demonstrated in the 3D-printed models, and there was good dispersion of ZrO₂ within the resin matrix. The impregnated resin remained UV curable and viscosity was not compromised. In this study, 3D-printed radiopaque features demonstrated clear radiopacity under X-ray and microcomputed tomography imaging.

Keywords: radiopacity, 3D printing, medical devices, additive manufacturing, nanoparticles, zirconium oxide

Introduction

3D PRINTING IS BECOMING MORE COMMON in health care and is expected to revolutionize personalized medicine in the coming years. ^{1,2} There was relatively little research on the use of 3D printing in the field of medicine before 2000, but this has increased significantly in recent years. ³ By way of example, 3D printing has already been utilized in orthopedics, ⁴⁻⁶ maxillofacial surgery, ⁷ cardiology, ⁸ neurology, ⁹ nephrology, ^{10,11} dentistry, ¹² and anesthesiology. ¹ The number of applications for 3D printing in medicine continues to grow, with many hospitals beginning to adopt this technology in laboratories located within hospitals. ¹³ To date, only a few cases of 3D-printed medical devices have been reported. ¹⁴ Currently, 3D printing in medicine is primarily used for surgical planning, custom-made surgical implants, as well as cutting guides for orthopedic applications. ^{3,6,15}

Utilizing medical scans to generate 3D-printed anatomical models has been reported multiple times ^{1,2,6,8,10,15,16–18} and these are ideal for explaining medical procedures to patients, ¹⁰ preoperative planning, and generating surgical guides. ^{6,15} Surgeons can use 3D-printed models to visualize complex anatomies such as vascular structures around organs. Such details can be difficult to visualize from 2D medical scans on a computer screen, but effortless with a 3D-printed model.

One of the limitations of 3D printing is lack of materials with different functional properties. ^{19–21} New materials have become available in recent years, but there is still a need to develop others with an even wider range of properties. Recent advances include flexible, transparent/opaque, biocompatible, and antimicrobial materials.

One limitation of materials for 3D printing is that the majority of polymers are not visible under X-ray imaging.²² Radiolucent refers to a material that is radiographically

Opposite page: Radiograph of two multi-material 3D printed hands with and without a novel radiologically accurate 3D printing resin. Photo credit: Dr. Aidan O'Sullivan and Dr. Julie O'Brien.

¹Design Factors Research Group, School of Design, University of Limerick, Limerick, Ireland.

²Radiology Department, University Hospital Limerick, Limerick, Ireland.

³Health Research Institute and Confirm Smart Manufacturing Centre, University of Limerick, Limerick, Ireland.

⁴School of Engineering, University of Limerick, Limerick, Ireland.

260 SHANNON ET AL.

translucent, and radiopaque refers to a material that is radiographically opaque. X-ray imaging, computed tomography (CT), and fluoroscopy all make use of differences in radiopacity to generate medical images. Visibility of stents and catheters on X-ray fluoroscopy can be difficult, and for this reason, radiopaque marker bands are often added to such devices. Gold, platinum, and tantalum are frequently used as markers on catheters due to their high radiopacity. Successful catheter insertion and stent deployment require the practitioner to know the exact location of the device within the patient's anatomy. A conventional 3D-printed polymer-based medical device would be difficult to view under X-ray imaging. A 3D printable radiopaque ink would improve visibility and increase opportunities for 3D printing of medical devices.

X-rays are ionizing radiation, meaning that they "knock" electrons from shells of atoms with which the X-rays interact. Elements of higher atomic number (symbol *Z*) result in greater attenuation of X-rays than elements of lower atomic number, due to the denser electron cloud. It is this attenuation of the X-rays that causes a material containing elements of higher atomic number to be more clearly visible on an X-ray detector. Radiopacity is measured in Hounsfield units (HU); air has the value of -1000 HU and water has the value of 0 HU.²⁴ Soft tissue has a radiopacity close to water with values between +40 HU and +100 HU.²⁴ Bone has a radiopacity in the range of +200 HU to in excess of +1000 HU.²⁴

Polymers generally contain elements of low atomic number, for example, carbon (Z=6) and hydrogen (Z=1), and are therefore radiolucent. Radiopaque elements have a higher atomic number, for example, gold (Z=79) and iodine (Z=53). Radiopaque material results in a visible region where the material lies between the X-ray source and detector. In a standard medical X-ray, bone shows up clearly on the detector, but soft tissues do not as they attenuate the X-ray signal less than bone.

Radiopaque 3D printing would be useful for practicing procedures on a realistic phantom before undertaking surgery on a patient. ¹⁹ For example, cardiac catheterization procedures could be performed using a 3D-printed phantom thorax, where the ribcage and spine are printed in a radiopaque material. The vertebrae serve as important landmarks during such procedures and would normally be invisible under fluoroscopy if printed using current materials. These phantoms could be printed to match the anatomy and varying radiological properties of the patient, ^{25,26} allowing better planning of procedures without risk to the patient. ²¹

3D-printed phantom anatomies with radiopaque properties would be useful to enhance medical training.²⁷ Medical scans of complex injuries, for example fractures, could be used to print exact replicas for training purposes. Medical imaging calibration aids are another potential application of phantoms with radiological properties. X-ray, fluoroscopy, or CT imaging could be calibrated from radiologically accurate 3D-printed anatomical models.

To make more realistic 3D-printed phantoms, radiopaque material would have to be modifiable to a variety of radiodensities, each corresponding to that of the different tissues within the body. This feature of combining materials is already possible on multimaterial PolyJet 3D printers, but radiopaque ink is not currently commercially available for this printing technology. Other nonink-based methods of radiopaque 3D printing include Fused Deposited Modeling printing, paper-based 3D printing, or loading 3D-printed components with radiopaque material postprinting.

PolyJet 3D printing has been used by other research groups to create phantoms such as a pelvis and a heart. ^{21,30} These were visually accurate but lacked realistic radiopacity. ^{21,30} Layers of gypsum bandages were applied to the pelvic phantom to represent cortical bone. ³⁰ Tantalum was glued to the cardiac phantom to represent regions of calcification. ²¹ Both research groups were aiming to improve radiopacity of the 3D-printed phantoms in the absence of a radiopaque ink for 3D printing.

In this study, zirconium oxide (ZrO_2) was chosen as the radiopaque additive as it is radiopaque and biocompatible. ^{31–33} As a result of these properties, ^{32–34} it has previously been used in dental applications ^{35–39} for restorations and fixed partial dentures. ⁴⁰

The purpose of this study was to develop an ultraviolet (UV) curable 3D printing resin. As part of this study, we printed a human hand model and a test block to test the capabilities of this material. Various properties of this material such as radiopacity, viscosity, thermal properties, and particle size were also evaluated.

Materials and Methods

3D printer and UV curable resins

An Objet Connex 500 multimaterial 3D printer (Stratasys Ltd., USA) was used for this study. This 3D printer uses PolyJet technology, which involves ink-jet printing UV curable photopolymer. The layer thickness for printing can be set at 16 or $32 \mu m$. The print heads heat the resin to 70° C, which reduces the viscosity, enabling the resin to be printed. There are two print heads for each material and two materials can be printed simultaneously. Each print head has 96 nozzles with a diameter of $50 \mu m$. Resin is deposited in layers on the print bed and cured with a high-intensity UV lamp. Each subsequent layer is deposited on top of the previously cured layer. Horizontal layers are built upward from the print bed until the final object is completed. Support material (SUP705; Stratasys, Ltd.) is printed to support overhanging structures and is removed through postprocessing using a high-pressure water jet cleaning station.

The photocurable acrylic resins used in this study were sourced from Stratasys, Ltd. When cured, Biocompatible Clear™ MED610 is a transparent rigid material, which has been developed for medical applications. Undoped MED610 was used as the base resin to develop radiopaque ink. Tango-BlackPlus™ FLX980 is a black rubber-like material when cured with shore hardness 27 (scale A). Multimaterial PolyJet technology is one of the few 3D printing techniques with the ability to print two or more materials at the same time. This multimaterial feature was essential during this study, as one cartridge was used for the radiopaque ink, and the other for a second material, TangoBlackPlus. As TangoBlackPlus is optically opaque, viewing the embedded radiopaque material was only possible under X-ray imaging, forming an ideal proof-of-concept experiment.

Radiopaque ink formulation and preparation

Assessment of ZrO₂ loading percentage. Disks of MED610 and various loading percentages of ZrO₂ were created to determine the minimum amount of additive required to produce visible radiopacity. Mixtures of 0.5, 1, 2, 5, 10, and 20 wt.% were manually mixed, cast, and then cured under UV lamps. All disks were X-rayed as described in the X-Ray Imaging section. Disk dimensions of diameter

10 mm and depth 2 mm were used in each case so that the radiopacity of each was comparable.

 $5\,\text{wt.}\%$ ZrO₂ radiopaque ink preparation. ZrO₂ nanopowder (544760-25G; Sigma Aldrich), with particle size $<100\,\text{nm}$, was used as received for this study. The radiopaque ink was combined in a ratio of $5\,\text{wt.}\%$ ZrO₂ to $95\,\text{wt.}\%$ MED610 resin.

The ZrO₂ nanopowder and MED610 were weighed individually in a fume hood fitted with a high-efficiency particulate air filter. The resin was continuously stirred using a magnetic stirrer while the ZrO₂ was added. The mixture was magnetically stirred for 30 min to fully immerse the powder within the resin, followed by mixing at 20,000 RPM using a high speed shear mixer (T 25 digital ULTRA-TURRAX; IKA Dispensers, Germany) for 10 min.

Dispersion stability of nanosized ZrO_2 in resin. For this study, it was essential that the ZrO_2 was dispersed well within MED610 and that it remained in suspension for at least 6 h to enable successful printing. If some ZrO_2 settled out of suspension during printing, the additive percentage would then be <5 wt.%.

Material characterization

Thermal ink characterization. Thermogravimetric analysis (TGA) was performed using a TGA 4000 (Perkin Elmer, USA). Undoped MED610 was heated to determine its decomposition temperature. After printing, TGA was carried out on the material remaining in the cartridge to assess if settling had occurred during printing, using undoped MED610 as a baseline. If settling occurs in the cartridge during printing, a larger mass than 5 wt. % would be detected.

While in the printer, the radiopaque ink may be subjected to multiple heating and cooling cycles. It was important to assess if the thermal history of the ink affected the behavior of the ink. For example, heating could cause portions of the resin to crystallize, which could block the print heads. Differential scanning calorimetry (DSC) was used to test if multiple heating/cooling cycles had a negative effect on the ink. DSC testing was performed using a DSC Polyma 214 (Netzsch, Germany). As the working temperature of the 3D printer is 70°C, the maximum temperature was set at 10°C greater than this. Minimum temperature was set as room temperature (20°C).

Ink viscosity characterization. Radiopaque inks of concentration 5, 10, 15, and 20 wt.% were tested to assess if the ink viscosity was affected by the introduction of ZrO_2 . Viscosity of undoped MED610 was also measured as a control. Viscosity measurements were performed using a DV3T Touch Screen Rheometer (Brookfield Ametek, USA). The viscosity was recorded at 70°C (working temperature) using a spindle size SC4-18. A shear rate ramp was used, starting at $66 \, \text{s}^{-1}$ and increasing in $33 \, \text{s}^{-1}$ increments until reaching $330 \, \text{s}^{-1}$.

Scanning electron microscopy on cured radiopaque ink. Particle dispersion and size distribution of ZrO_2 in the 3D-printed samples was analyzed visually using a scanning electron microscope (SEM; Helios G4 CX; Thermo Fisher Scientific/FEI, USA). Fracture surfaces of the samples were imaged to assess if agglomeration of the ZrO_2 particles had

occurred or if they were dispersed as uniformly distributed single particles.

Imaging of the radiopaque 3D-printed samples

X-ray imaging. All radiographs were imaged at the University Hospital Limerick using a DRX-Evolution X-ray system (Carestream Health, USA), with a source voltage of 52 kVp, exposure of 1.8 mAs, and a focal distance of 110 cm between the tube and the sample for all scans. All radiographs were analyzed using McKesson Radiology Software (McKesson Enterprise Medical Imaging, Ireland).

The Test Method Standard ASTM F640-12⁴¹ was used to assess the radiopacity of the 3D-printed samples. As per the standard, a step wedge of known radiopacity for each step was included as a reference during all X-ray imaging, to ensure that all images were comparable.

Microcomputed tomography. All microcomputed tomography (microCT) scans for this project were taken on an Xradia VersaXRM-500 (ZEISS, Germany). X-ray source voltage was 80 keV and camera temperature was -59°C for all scans. The 3D models were scanned in 2D segments, which were later combined using XM3DViewer 1.2.8 software to create the 3D file for visualization purposes (Supplementary Video S1).

3D-printed models

To explore a range of capabilities of the radiopaque ink, two 3D models containing different geometric features were printed; a model of a human hand (Fig. 1A) and a test block (Fig. 1B). The hand was printed from an STL file (provided by Stratasys, Ltd. as a demonstration model and derived from anonymized CT scan data). A solid test block comprising different geometrical shapes internally was designed using computer-aided design (CAD) software (SolidWorks 2018; Dassault Systèmes, France).

The 3D model of the hand was printed to test the capabilities of the radiopaque ink in such anatomical phantoms. The bones of the hand were printed with radiopaque ink and the soft tissue was printed with TangoBlackPlus. A control hand was also produced with bones printed in undoped MED610.

The test block was designed with a range of internal shapes of varying sizes and thicknesses. Hollow cylindrical shapes were included to assess how catheters or guidewires might appear if made from this radiopaque ink. Overlapping disks were included to confirm that higher radiopacity could be achieved in areas where there was a thicker cross section of radiopaque material between the X-ray source and detector. Cuboids of the same height and length but varying thickness were included to test and demonstrate the resolution of the print.

Results

Radiopaque ink formulation and preparation

Assessment of ZrO_2 loading percentage. Manually cast and cured disks of ZrO_2 and MED610 resin showed a linear radiopacity increase with increasing ZrO_2 content from 0.5 to 20 wt.%, with an R^2 value of 0.99, as seen in Figure 2A. Disks with ZrO_2 concentration <5 wt.% did not show much increase in radiopacity compared with undoped MED610, as shown in Figure 2A. However, 5 wt.% showed an increase of radiopacity at a relatively low loading percentage. Since the loading

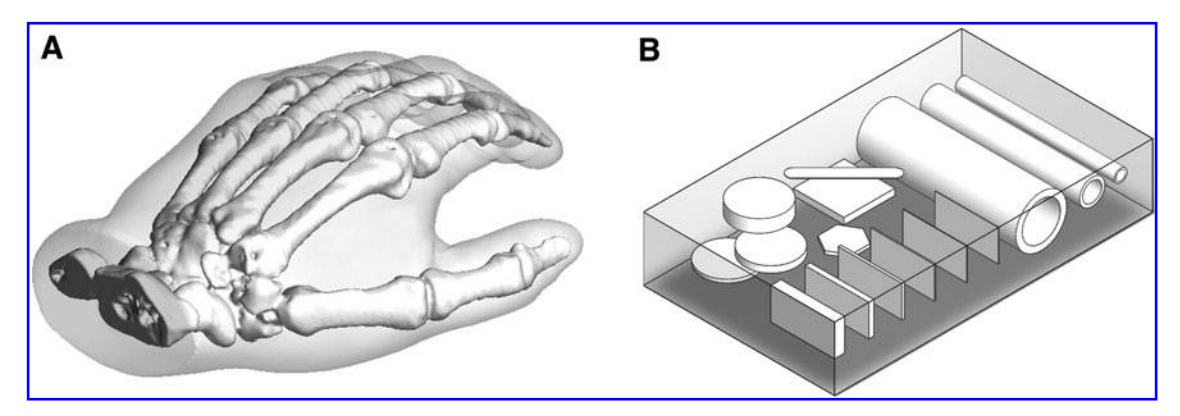


FIG. 1. (A) The 3D CAD model of the hand model. (B) The 3D CAD model of the test block. CAD, computer-aided design.

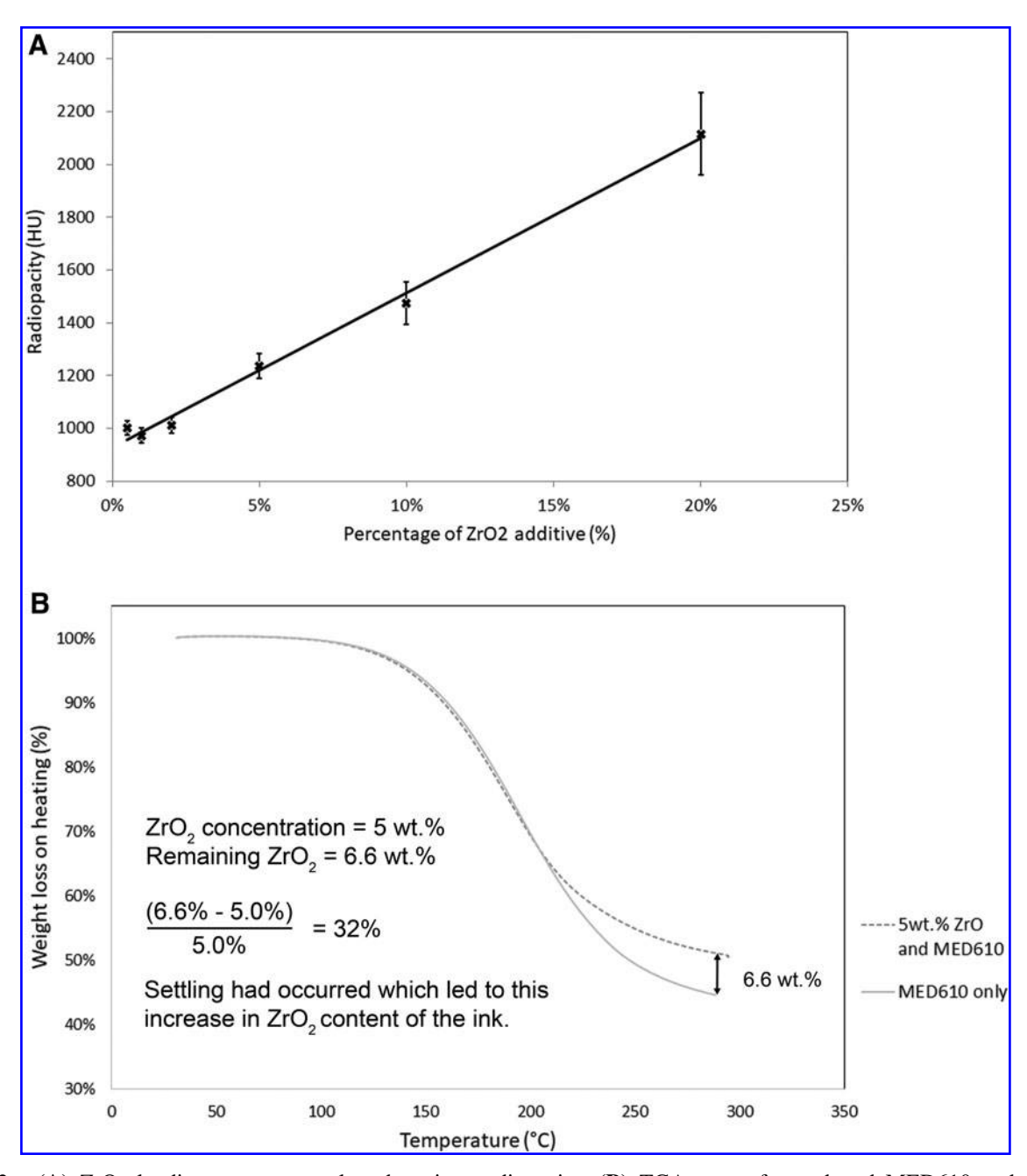


FIG. 2. (A) ZrO_2 loading percentage plotted against radiopacity. (B) TGA curve for undoped MED610 and 5 wt.% radiopaque ink collected after 3D printing had taken place to evaluate the degree of settling that takes place during the printing process. HU, Hounsfield units; TGA, thermogravimetric analysis; ZrO_2 , zirconium oxide.

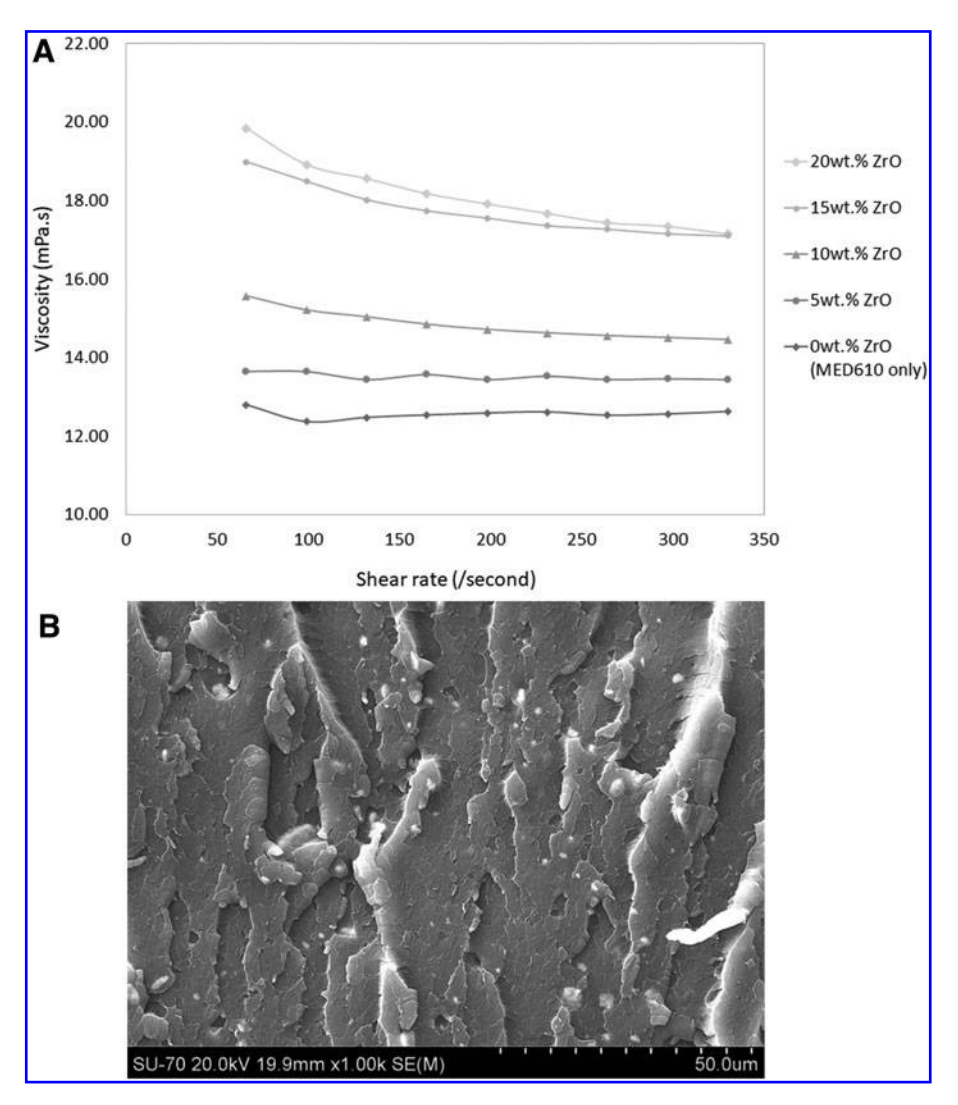


FIG. 3. (A) Viscosity versus shear rate is plotted for different loading percentages of ZrO_2 (at 70°C). (B) SEM image of MED610 with ZrO_2 fracture surface to show that agglomerates >5 μ m were not forming. SEM, scanning electron microscope.

percentage was still quite low, the printability was not compromised (see the viscosity results Ink Viscosity Characterization section).

 $5\,\text{wt.}\%\,\text{ZrO}_2$ ink preparation. After shear mixing, the ZrO_2 was dispersed well within MED610 resin. The resin containing nanoparticles remained stable at room temperature for 6–8 h after mixing, which presented a workable duration for printing. After this duration, some ZrO_2 settled to the bottom of the container, which required reagitation by shear mixing.

The uncured radiopaque ink had a gray-lilac color. When cured, the radiopaque ink had a light gray color.

Material characterization

Ink thermal characterization. The TGA curve in Figure 2B shows a 6.6 wt.% difference between undoped MED610 and of the radiopaque ink that remained in the cartridge after printing had taken place. As the ZrO₂ concentration should have been 5 wt.%, it is understood that 32% of ZrO₂ settled out of suspension during 3D printing, resulting in the higher than expected ZrO₂ content in the cartridge after printing had taken place.

Multiple DSC heating/cooling cycles, between 20°C and 80°C, demonstrated that there was no crystallization or other

notable thermal features with repeated heating and cooling of the radiopaque ink. This ensured that any blockages in the print heads were not due to crystallized ink.

Ink viscosity characterization. Undoped MED610 had a viscosity of ~ 12.6 mPa.s at 70°C, and the 5 wt.% radiopaque ink had a viscosity of ~ 13.5 mPa.s at 70°C, as shown in Figure 3A. Viscosity was increased by 0.94 mPa.s on average with the addition of $\rm ZrO_2$. Thus, the original rheological properties of the ink were not compromised.

Scanning electron microscopy. SEM confirmed that there was a good level of dispersion of ZrO_2 within the printed parts (Fig. 3B). No agglomerates >5 μ m were observed.

Radiopacity of 3D-printed models

Good radiopacity was achieved in the 3D-printed radiopaque models, as seen in Figure 4 below.

X-ray imaging. A photograph and radiograph of the 3D-printed hands are shown in Figure 4A; the left hand is of the control with the bones printed in undoped MED610, and the right hand containing bones printed with the radiopaque ink. The hands are indistinguishable in the photograph, whereas the radiopaque bones are clearly visible on the radiograph.

264 SHANNON ET AL.

Regions of overlapping bone in Figure 4A-ii displayed higher levels of radiopacity where there was a greater cross section of radiopaque material. The undoped MED610 bones in the control hands are completely invisible in the X-ray image.

Photographs of the test block X-ray setup are shown in Figure 4B-i and C-i. X-ray images of the test block are shown in Figure 4B-ii and C-ii. The radiopaque aluminum reference step wedge is included, as per the ASTM F640-12.⁴¹

The resolution of the 3D-printed radiopaque features was very good—with a feature of thickness $100 \,\mu\text{m}$ visible in Figure 5B. The control block did not show any of the internal features.

Microcomputed tomography. Figure 5A shows slices of the microCT imaging of the hand with the bones printed with radiopaque ink. The slice location is highlighted in Figure 5A-ii. This demonstrates how successful the radiopaque 3D printing had been. While X-ray imaging confirmed that radiopaque particles had successfully printed, microCT showed the finer details, such as the printed layers and the homogeneity of the print.

Figure 5A-i shows streaky layers that are not parallel with the build tray. These streaks of varying radiopacity were visible under microCT imaging, but not under 2D X-ray imaging due to the orientation and resolution of the X-ray image.

Figure 5B-i shows the test block in plan view. The dotted line represents the microCT cross section where the $100 \,\mu m$ feature is visible. This 2D microCT slice is shown in Figure 5B-ii and B-iii. The dimensions of this feature were

confirmed by plotting grayscale values against dimensions. The profile shown in Figure 5B-iv confirms that the thickness of the smallest feature is $\sim 200~\mu m$. Since the CAD model of this feature measured $100~\mu m$, this is accurate and within the tolerance of $100~\mu m$ as stated by the manufacturer.

Discussion

Currently, research groups are adding radiopaque material in postprinting processes to improve the radiopacity of phantoms. ^{21,30} It has been detailed in the literature that there is no radiopaque ink available for Stratasys Polyjet 3D printers, ⁴² which are commonly used in hospital settings.

This proof-of-concept study describes a method to create a radiopaque UV curable ink suitable for 3D printing radiopaque artifacts. Our method has demonstrated that features as low as $100~\mu m$ in resolution can be printed and are clearly visible under X-ray imaging. The 3D printing resin remained UV curable and the viscosity was not considerably altered with the addition of 5 wt.% ZrO₂. MED610 has a viscosity of 12.6 mPa.s and this value increased slightly to 13.5 mPa.s with the addition of 5 wt.% ZrO₂. In addition to this, no agglomerates >5 μm were observed when the material was viewed under SEM. 5 wt.% ZrO₂ allows a greater radiopacity to be produced with less material, allowing better visibility, without compromising printability.

As part of this study, we 3D printed a model of a human hand and a test block, both with internal radiopaque features. The bones printed with this radiopaque ink are clearly visible under

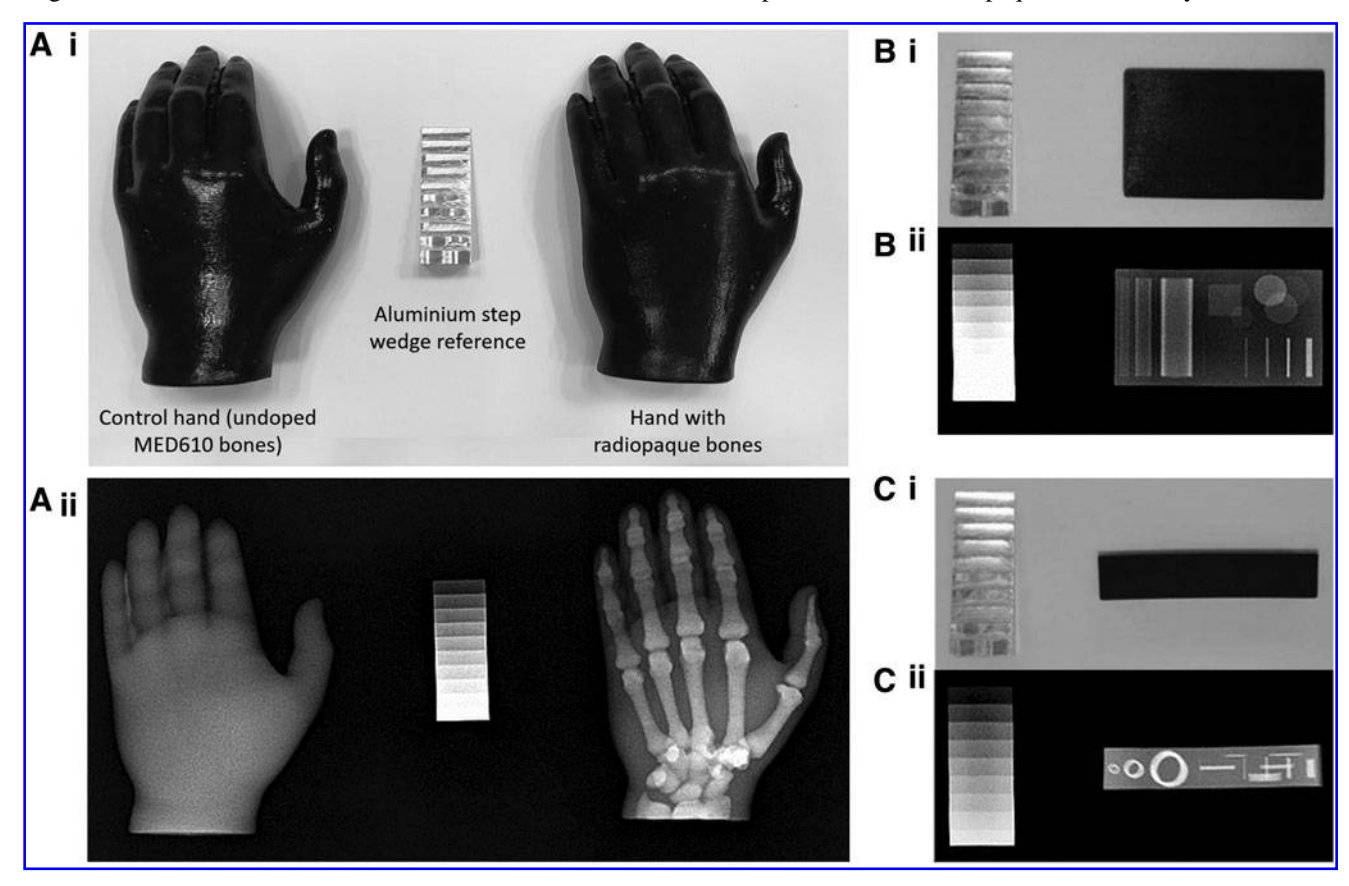


FIG. 4. (A) The 3D-printed hand on the *left* of the image contains bones that were printed with undoped MED610 and the hand on the *right* of the image contains bones printed with radiopaque ink. (A-i) Photograph of both 3D-printed hands. (A-ii) Radiograph of both 3D-printed hands. (B-i) Photograph of the test block in plan view. (B-ii) Radiograph of the test block in plan view. (C-i) Photograph of the test block in side view. (C-ii) Radiograph of the test block side view. The aluminum step wedge is included in the images as per ASTM F640-12.

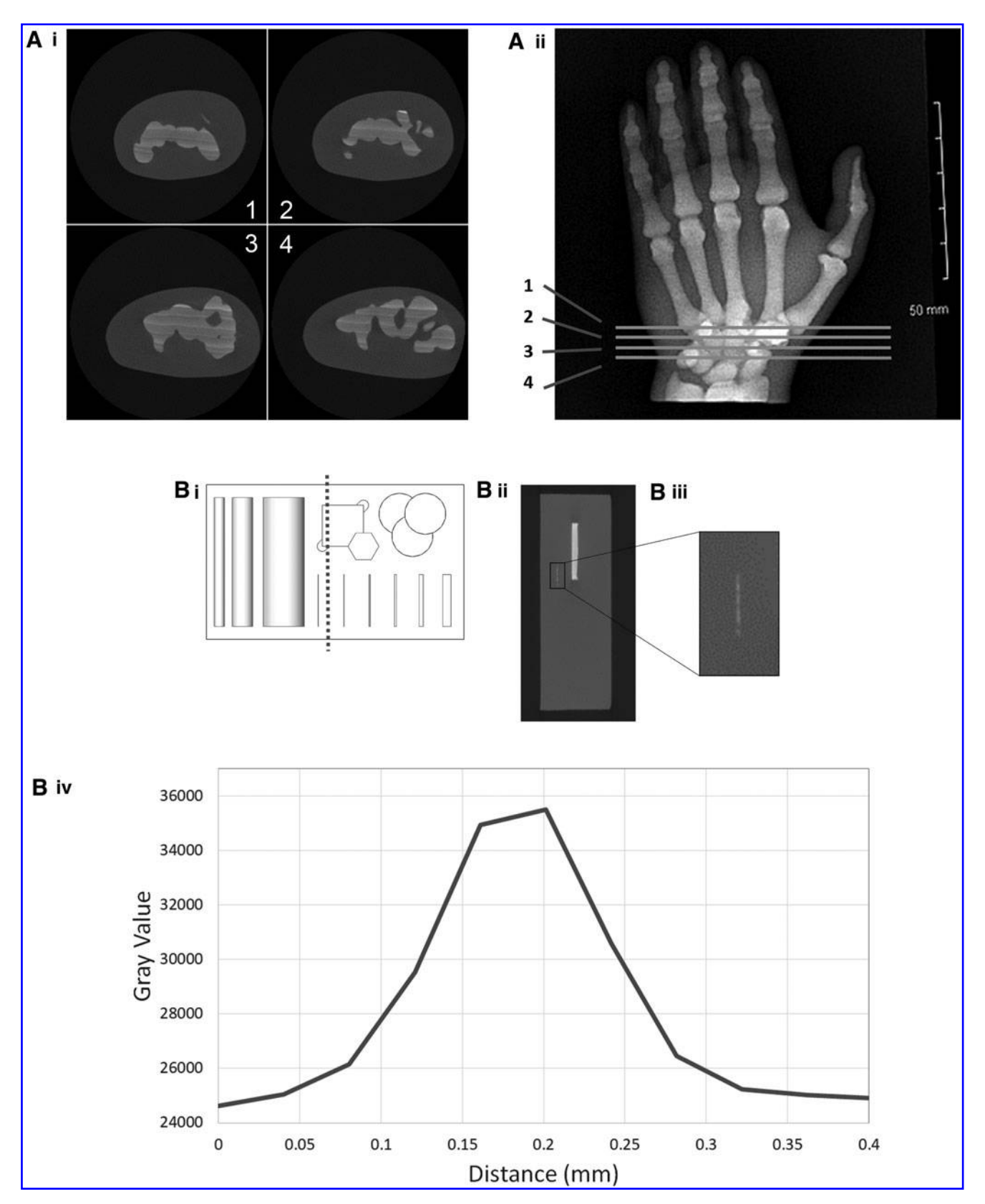


FIG. 5. (A-i) Four individual microCT slices of the hand printed with radiopaque bone as the internal features. (A-ii) The four slices from (A-i) are highlighted on the X-ray of the hand. (B-i) The microCT cross section of the test block is highlighted by the *dotted line*. (B-ii) The microCT cross section of the test block. The smallest feature of this model is highlighted in a *black box* and enlarged in the next image. (B-iii) The expanded view of the smallest radiopaque feature of the test block. The smaller *white horizontal line* is the section that is profiled in the graph. (B-iv) The profile of the smallest feature is plotted as grayscale against dimensions to evaluate actual dimensions of this feature. microCT, microcomputed tomography.

266 SHANNON ET AL.

X-ray imaging, with higher radiopacity in thicker regions as would be expected for real bone. Using the same method, other anatomies such as a cranial model or thorax could be printed and would mimic the original under X-ray imaging. This is an important step for 3D printing as more realistic phantoms could be used for medical training or to improve surgical planning. This material can be used to enhance the realism of simulation for medical training purposes. Although the print was successful, the model of the hand was limited by the original scan segmentation—the bones were segmented as solid, rather than accounting for the inner trabecular structure of the bone. The internal features of the test block show hollow cylinders and overlapping disks that are visible under X-ray imaging. The hollow cylinders demonstrate how a catheter would appear if printed with this material. This is a fundamental step on the road to 3D printing complete medical devices. The test block is an example of how radiopaque 3D printing could be used to generate calibration aids for X-ray, CT, or fluoroscopy. Shapes of known geometry and radiopacity could be printed for performing calibration of these imaging modalities.

A limitation of this study is that the ZrO₂ is settling, which results in some nozzles becoming blocked during printing. The settling and blocked nozzles both contributed to nonplanar layers and varying radiopacity as observed in the cross section of the hand. The print head takes in only enough material to print the next number of layers, causing material to move in a pulsatile manner along the printer tubing rather than a steady flow of material. This allows time for the material to settle, which could be responsible for the periodic fluctuations in radiopacity seen in the hand cross section. Even though the material was stable for 6h at room temperature, settling was accelerated at 70°C in the print head. In addition, the printer purges approximately every 180 layers, depending on the material and printing mode. The printer purges at a high velocity to clear any blockages from the nozzle, and this may also contribute to the periodic increases in radiopacity. The settling issues and print head blockages will need to be resolved before these radiopaque models are used for any diagnosis or surgical planning. The actual radiopacity of models versus patients' anatomy under medical imaging will need to be validated further as part of future research.

Layers that were not parallel to the build tray were due to blocked nozzles. Less material is deposited where the nozzle is blocked, resulting in partial layers being printed. This accrues with each layer, as the previous nonparallel layer becomes the foundation for the next.

According to the Connex 500 user manual, a significant blockage is "more than 10 missing lines in one area." After each radiopaque print, a pattern test was performed to test for blockages. If significant blockages were observed, then the print head was removed and flushed with isopropanol to remove any excess ZrO₂ particles that had accumulated in the print head.

Other studies that added radiopaque material to the outside of printed models^{21,30} did not encounter the same issues with settling and blocked print heads, but arguably did not achieve the same quality of results. The method described in this study is a step toward 3D printing radiopaque medical devices without the additional postprinting step to improve visibility. The radiopaque ink in the cartridge remained stable while printing and required agitation after 6 h, which was acceptable as the hand took 4 h to print. TGA highlighted that up to 32% settling occurred during printing, and we will aim

to reduce this value by chemically treating the ZrO₂ particle surface with suitable surfactants.

Further experiments are required to evaluate if surfactants could create a more stable suspension of ZrO₂ within MED610 to reduce settling and nozzle blockages. Future work will need to be performed to keep ZrO₂ in suspension for a longer duration. Reducing nozzle blockages and keeping particles in suspension for longer would greatly improve the print quality and allow larger models to be produced. This research involved using the 3D printer in ways that the manufacturer would not have anticipated, and may therefore invalidate current warranties if in place. More research is required to investigate potential effects due to using the modified material.

Conclusions

To the best of our knowledge, this is the first functional radiopaque ink for Polyjet 3D printing. A model of a human hand with radiopaque bone and a test block were successfully printed with features as low as $100 \, \mu \text{m}$ in resolution. X-ray imaging demonstrated successful printing of radiopaque features within the models. This method was successful using the Stratasys Objet Connex 500 multimaterial 3D printer, and may be adapted to suit other 3D printing technologies.

Acknowledgments

The authors further acknowledge the people responsible for providing training, equipment, and/or assisting with measurements. 3D printing: Mr. Donal Ryan, Rheology: Mr. Leo Kirby, DSC/TGA: Dr. Wynette Redington, SEM: Ms. Paula Olsthoorn and Dr. Robbie O'Connell, Mechanical testing: Mr. Clive Considine and Mr. Adrian McEvoy.

Author Disclosure Statement

No competing financial interests exist.

Funding Information

This publication has emanated from research supported, in part, by the Irish Research Council and National Children's Research Centre, and a research grant from the Science Foundation Ireland (SFI) under Grant Number SFI 16/RC/3918 (CONFIRM Smart Manufacturing Research), cofunded by the European Regional Development Fund.

Supplementary Material

Supplementary Video S1

References

- Gálvez JA, Simpao AF, Dori Y, et al. Not just a pretty face: Three-dimensional printed custom airway management devices. 3D Print Addit Manufact 2016;3:160–165.
- Honigmann P, Sharma N, Okolo B, et al. Patient-specific surgical implants made of 3D printed PEEK: Material, technology, and scope of surgical application. BioMed Res Int 2018;2018:8.
- 3. Tack P, Victor J, Gemmel P, *et al.* 3D-printing techniques in a medical setting: A systematic literature review. Biomed Eng Online 2016;15:115.
- Mulford JS, Babazadeh S, Mackay N. Three-dimensional printing in orthopaedic surgery: Review of current and future applications. ANZ J Surg 2016;86:648–653.

- 5. Frame M, Huntley JS. Rapid prototyping in orthopaedic surgery: A user's guide. Sci World J 2012;2012:7.
- Auricchio F, Marconi S. 3D printing: Clinical applications in orthopaedics and traumatology. EFORT Open Rev 2016;1:121–127.
- Saijo H, Igawa K, Kanno Y, et al. Maxillofacial reconstruction using custom-made artificial bones fabricated by inkjet printing technology. J Artific Organs 2009;12:200–205.
- Valverde I, Gomez G, Coserria JF, et al. 3D printed models for planning endovascular stenting in transverse aortic arch hypoplasia. Catheter Cardiovasc Interv 2015;85:1006–1012.
- Randazzo M, Pisapia JM, Singh N, et al. 3D printing in neurosurgery: A systematic review. Surg Neurol Int 2016; 7(Suppl. 33):801–809.
- Bernhard J-C, Isotani S, Matsugasumi T, et al. Personalized 3D printed model of kidney and tumor anatomy:
 A useful tool for patient education. World J Urol 2016;34:337–345.
- 11. Kusaka M, Sugimoto M, Fukami N, *et al.* Initial experience with a tailor-made simulation and navigation program using a 3-D printer model of kidney transplantation surgery. Transplantat Proceed 2015;47:596–599.
- 12. Hayden HC. Exploration of materials used in 3-dimensional printing for the dental industry, in W.M. Keck Science Department. 2015: Scripps Senior Theses.
- Abdullah KA, Reed W. 3D printing in medical imaging and healthcare services. J Med Radiat Sci 2018;65:237–239.
- O'Sullivan KJ, O'Sullivan AG, Power N, et al. Use of 3D printing to create a bespoke repair of a Percutaneous Endoscopic Gastrostomy (PEG) tube in patient unfit for surgical replacement. BMJ Innovat 2018;4:29–31.
- Giannopoulos AA, Steigner ML, George E, et al. Cardiothoracic applications of 3D printing. J Thorac Imag 2016;31:253.
- Jahnke P, Schwarz S, Ziegert M, et al. Paper-based 3D printing of anthropomorphic CT phantoms: Feasibility of two construction techniques. Eur Radiol 2019;29:1384–1390.
- Hamedani BA, Melvin A, Vaheesan K, et al. Threedimensional printing CT-derived objects with controllable radiopacity. J Appl Clin Med Phys 2018;19:317–328.
- 18. Jahnke P, Limberg FR, Gerbl A, *et al.* Radiopaque three-dimensional printing: A method to create realistic CT phantoms. Radiology 2016;282:569–575.
- 19. Vukicevic M, Mosadegh B, Min JK, *et al.* Cardiac 3D printing and its future directions. JACC: Cardiovasc Imag 2017;10:171–184.
- Gear JI, Cummings C, Craig AJ, et al. Abdo-Man: A 3Dprinted anthropomorphic phantom for validating quantitative SIRT. EJNMMI Phys 2016;3:17.
- Izzo RL, O'Hara RP, İyer V, et al. 3D printed cardiac phantom for procedural planning of a transcatheter native mitral valve replacement. Proc SPIE Int Soc Opt Eng 2016;9789:978908.
- Chadwick B, Toto C. Radiolucent structural materials for medical applications. Med Device Diagnost Industry 2001;23:40–48.
- Létourneau-Guillon L, Soulez G, Beaudoin G, et al. CT and MR imaging of nitinol stents with radiopaque distal markers. J Vasc Intervent Radiol 2004;15:615–624.
- Broder J, Preston R. Diagnostic Imaging for the Emergency Physician, ed. J. Broder. Amsterdam, The Netherlands: Elsevier Health Sciences, 2011.
- Li J, Zhong Z, Lidtke R, et al. Radiography of soft tissue of the foot and ankle with diffraction enhanced imaging. J Anatomy 2003;202:463–470.

- Edmonds M, Morrison N, Laws J, et al. Medial arterial calcification and diabetic neuropathy. Br Med J (Clin Res Ed) 1982;284:928–930.
- Laing J. A patient-specific cardiac phantom for training and pre-procedure surgical planning. Electronic thesis and dissertation repository, 4964, 2017.
- Filippou V, Tsoumpas C. Recent advances on the development of phantoms using 3D printing for imaging with CT, MRI, PET, SPECT, and ultrasound. Med Phys 2018;45:740–760.
- Boyer CJ, Ballard DH, Weisman JA, et al. Threedimensional printing antimicrobial and radiopaque constructs.
 Print Addit Manufact 2018;5:29–36.
- Niebuhr NI, Johnen W, Güldaglar T, et al. Radiological properties of tissue surrogates used in a multimodality deformable pelvic phantom for MR-guided radiotherapy. Med Phys 2016;43:908–916.
- 31. Bona AD, Pecho OE, Alessandretti R. Zirconia as a dental biomaterial. Materials 2015;8:4978–4991.
- 32. Fonseca RB, Branco CA, Soares PV, *et al.* Radiodensity of base, liner and luting dental materials. Clin Oral Invest 2006;10:114–118.
- 33. Pekkan G. Radiopacity of dental materials: An overview. Avicenna J Dent Res 2016;8:e36847.
- 34. Taira M, Toyooka H, Miyawaki H, *et al.* Studies on radiopaque composites containing ZrO2 ☐ SiO2 fillers prepared by the sol-gel process. Dental Mater 1993;9:167–171.
- 35. Attar N, Tam LE, McComb D. Mechanical and physical properties of contemporary dental luting agents. J Prosthet Dentistry 2003;89:127–134.
- 36. Guerreiro-Tanomaru JM, Cornélio ALG, Andolfatto C, *et al.* pH and antimicrobial activity of Portland cement associated with different radiopacifying agents. ISRN Dentistry 2012;2012 DOI: 10.5402/2012/469019.
- 37. Nistor L, Grădinaru M, Rîcă R, *et al.* Zirconia use in dentistry-manufacturing and properties. Curr Health Sci J 2019;45:28.
- 38. Ban S. Reliability and properties of core materials for all-ceramic dental restorations. Jpn Dental Sci Rev 2008;44:3–21.
- 39. Pekkan G, Pekkan K, Hatipoglu MG, *et al.* Comparative radiopacity of ceramics and metals with human and bovine dental tissues. J Prosth Dentistry 2011;106:109–117.
- Atsu SS, Kilicarslan MA, Kucukesmen HC, et al. Effect of zirconium-oxide ceramic surface treatments on the bond strength to adhesive resin. J Prosth Dentistry 2006;95:430–436.
- 41. ASTM, ASTM F640-12, Standard Test Methods for Determining Radiopacity for Medical Use. West Conshohocken, PA: ASTM International, 2012.
- 42. Meess KM, Izzo RL, Dryjski ML, *et al.* 3D printed abdominal aortic aneurysm phantom for image guided surgical planning with a patient specific fenestrated endovascular graft system. Proc SPIE Int Soc Opt Eng 2017;10138:101380P.
- 43. Connex500/350 3D printer system, in User Manual, S. Ltd., Editor. 2014, Stratasys Ltd: Eden Prairie, MN.

Address correspondence to:

Leonard O'Sullivan

Design Factors Research Group

School of Design

University of Limerick

Foundation Building

Limerick V94 PX58

Ireland

E-mail: leonard.osullivan@ul.ie